

Journal of Materials Chemistry A

Accepted Manuscript



This is an *Accepted Manuscript*, which has been through the Royal Society of Chemistry peer review process and has been accepted for publication.

Accepted Manuscripts are published online shortly after acceptance, before technical editing, formatting and proof reading. Using this free service, authors can make their results available to the community, in citable form, before we publish the edited article. We will replace this *Accepted Manuscript* with the edited and formatted *Advance Article* as soon as it is available.

You can find more information about *Accepted Manuscripts* in the [Information for Authors](#).

Please note that technical editing may introduce minor changes to the text and/or graphics, which may alter content. The journal's standard [Terms & Conditions](#) and the [Ethical guidelines](#) still apply. In no event shall the Royal Society of Chemistry be held responsible for any errors or omissions in this *Accepted Manuscript* or any consequences arising from the use of any information it contains.

ARTICLE

Flexible nanocomposites with enhanced microwave absorption properties based on Fe₃O₄/SiO₂ nanorods and polyvinylidene fluoride

Cite this: DOI: 10.1039/x0xx00000x

Xiaofang Liu,^a Yaxin Chen,^a Xinrui Cui,^a Min Zeng,^a Ronghai Yu^a and Guang-Sheng Wang^{*b}

Received 00th January 2012,

Accepted 00th January 2012

DOI: 10.1039/x0xx00000x

www.rsc.org/

The Fe₃O₄/SiO₂ porous nanorods with one-dimensional core/shell structure and high aspect ratio have been synthesized as an absorber by a wet chemical method. Based on the nanorods, flexible Fe₃O₄/SiO₂/PVDF nanocomposites have been firstly prepared by embedding the Fe₃O₄/SiO₂ nanorods in polyvinylidene fluoride (PVDF) matrix. The Fe₃O₄/SiO₂/PVDF nanocomposite with filler content of 40 wt.% shows excellent microwave absorption performance over 2–18 GHz, and the minimum reflection loss (RL) can reach –28.6 dB as the thickness is 2.5 mm. The mechanisms for the enhanced microwave absorption performance were clarified based on the unique structural features as well as the synergetic effect between multiple components.

1. Introduction

With the rapid development of wireless communication and the wide applications of electronic devices, electromagnetic (EM) interference and EM radiation have become serious environmental pollutions resulting in great harm to electromagnetic compatibility, information safety and human health.^{1–3} Extensive researches have been therefore devoted to developing high-performance microwave absorption materials with the advantages of strong absorption, wide absorption frequency, high thermal stability, lightweight and antioxidation.^{4–6} Over the past decades, magnetite (Fe₃O₄), which is a typical double-complex medium with dielectric loss and magnetic loss, has attracted considerable interest in EM interference shielding and EM wave absorption applications because of its low cost and strong absorption.⁷ However, general Fe₃O₄ particles used as the fillers in microwave absorbers have shortcomings of permeability drop caused by Snoek's limit at high frequency, narrow absorption frequency range (mainly distributing in low frequency range), high density (addition amount is over 50 wt.%), and ease of oxidation.⁸

Recently, many efforts have focused on improving the microwave absorption performance of the Fe₃O₄ materials. Especially, the progresses in synthesis of nanomaterials promote the fast development of Fe₃O₄ microwave absorbers with various special and complex nanostructures. Considering the impedance matching problem, the Fe₃O₄ nanocomposites with core-shell or yolk-shell architectures have been extensively studied. By selectively coating inorganic or organic shell, such composites based on Fe₃O₄ nano- and micron-sized spheres have shown great potential as microwave absorbers with lower reflection loss and wider absorption frequency range

than single-component Fe₃O₄ counterparts. At the same time, the formed shell could provide heterointerface to enhance absorption properties and protect the inner Fe₃O₄ core from environmental oxidation. Until now, a variety of core-shell/yolk-shell Fe₃O₄ nanospheres/microspheres, such as Fe₃O₄/TiO₂,⁴ Fe₃O₄/SnO₂,⁹ Fe₃O₄/ZnO¹⁰ and Fe₃O₄/polyaniline,¹¹ have been successfully prepared and exhibited promising microwave absorption performance at GHz frequency range.

In addition to designing core-shell/yolk-shell structures, fabrications of one dimensional (1D) nanomaterials and porous nanostructures are also alternative methods to obtain high-performance microwave absorbers. In theory, the large anisotropy of 1D nanomaterials may enable Fe₃O₄ to overcome the problem of comparatively small intrinsic anisotropy, leading to larger permeability and higher resonance frequency over the Snoek's limit in GHz frequency range. Nowadays, the advantages of 1D nanomaterials used for microwave absorbers have been proved by many groups. Zhu et al. synthesized Fe₃O₄ nanorod array/graphene architecture which can attenuate more than 99% of EM wave energy in GHz frequency range.¹² Yan et al. fabricated Fe₃O₄ nanowires via a NaAc-assisted coprecipitation method and obtained the minimum reflection loss of –16.67 dB at 8.32 GHz.¹³ Moreover, recent studies showed that the introduction of pores in the microwave absorption materials can simultaneously enhance the microwave absorption property and reduce the density of the powders.¹⁰ If vacancies and pores are present in the absorbers, the incident EM wave could be repeatedly reflected and scattered inside the porous structures, which are beneficial for the attenuation of EM wave. For instance, porous α -Fe₂O₃ nanospheres, porous Fe₃O₄-decorated graphene as well as mesoporous Fe₃O₄/ZnO spheres decorated graphene have been

studied and considered as lightweight and high efficiency microwave absorbers.^{10, 14, 15}

Although many Fe₃O₄ microwave absorbers with special and complex nanostructures have been extensively studied in the recent five years, the materials are still at early research stage, and the relationships between structure and improved performance need to be further clarified. In this study, we report a novel nanocomposite absorber based on polyvinylidene fluoride (PVDF) and synthesized Fe₃O₄/SiO₂ porous nanorods. Such Fe₃O₄/SiO₂ nanorods combine various structural advantages for high-performance microwave absorbers together, i.e. core-shell structure, 1D nanorods with high aspect ratio, and porous structures containing numerous pores and cavities. Besides, the coated SiO₂ wave-transparent shell is beneficial for adjusting impedance matching and can effectively protect the inner Fe₃O₄ nanorod against oxidation. Meanwhile the coating of SiO₂ shell has exceptional advantages of easy preparation and low cost. Here, we used PVDF polymer instead of conventional paraffin as dispersed matrix. On one hand, the synergetic effect between nanorods and dielectric matrix may be helpful for enhancing absorption abilities.^{16, 17} On the other hand, the characteristics of low weight, high chemical corrosion resistance and heat resistance for PVDF are favorable to the practical applications of the absorbers. More interestingly, the flexible feature of PVDF matrix endows the Fe₃O₄/SiO₂/PVDF nanocomposite excellent flexibility, which would immensely expand the applications of the absorber; especially it may be useful in the materials and devices with transformable or extremely complicated structures. The synthesized Fe₃O₄/SiO₂/PVDF nanocomposite exhibits strong microwave absorption performance with the advantages of light weight, antioxidation and flexibility. The mechanisms via unique structural characters as well as the synergetic effect between multiple components to enhance microwave absorption are also discussed.

2. Experimental

2.1. Sample preparation

All reagents are of analytical grade and used without further purification.

Synthesis of FeOOH nanorods: The synthesis of FeOOH nanorods is based on a previous report.¹⁸ Typically, 0.6 M of FeCl₃·6H₂O was dissolved in 500 mL of H₂O. The solution was added in 0.07 M of 37% HCl and then stirred for 20 min. The mixture solution was stored in 500 mL Schott bottle and aged in an oven at 98 °C for 24 h. After cooling down to room temperature, the precipitates were collected by centrifugation and washed with water for several times.

Silica coating of FeOOH nanorods: The above FeOOH nanorods were redispersed in 200 mL of H₂O, and 10 mL of PAA (0.1 M) solution was added for the surface modification of nanorods. After overnight stirring, the nanorods were collected by centrifugation and were redispersed in 180 mL of H₂O. Subsequently, 6 mL of ammonia solution and 160 mL of ethanol were added to the suspension. Under magnetic stirring, a certain amount of TEOS was injected to the mixture for silica coating. After 1 h, the silica-coated nanorods were collected by centrifugation, washed with water for several times and dried at 60 °C for 24 h.

Conversion of FeOOH/SiO₂ nanorods to Fe₃O₄/SiO₂ nanorods: The Fe₃O₄/SiO₂ nanorods were produced by annealing the as-prepared FeOOH/SiO₂ nanorods at 400 °C for

1 h under a continuous H₂/N₂ gas flow (5% H₂). After H₂ reduction, the color of the sample changed from yellow to black.

Preparation of Fe₃O₄/SiO₂/PVDF nanocomposite: The above Fe₃O₄/SiO₂ nanorods (40 wt.%) were ultrasonically dispersed in 30 mL of DMF for 1 h, followed by addition of PVDF into the suspension. After stirring for 60 min at room temperature and ultrasonication for another 1 h, the mixture was poured into a glass plate to form a thin film, and then dried in oven.

2.2. Structural characterization

The crystal structure of the samples was analyzed using x-ray diffractometer (XRD, D/MAX-1200, Rigaku Denki Co. Ltd., Japan) with Cu K α irradiation at $\lambda=0.15406$ nm. Transmission electron microscopy (TEM, JEOL-2100F) and field emission scanning electron microscopy (JSM-7500F) were used to observe the morphology, size and microstructure of the samples. X-ray photoelectron spectroscopy (XPS) was recorded using a spectrometer with Mg K α radiation (ESCALAB 250, Thermofisher Co.) for composition determination. Room-temperature magnetic properties of the sample were measured by lakeshore vibrating sample magnetometer (VSM).

2.3. Measurement of microwave absorption performance

The electromagnetic parameters of the Fe₃O₄/SiO₂/PVDF nanocomposites were measured by the transmission/reflection coaxial line method. The sample for testing were compacted into a cylindrical shaped compact ($\Phi_{\text{out}}=7.00$ mm and $\Phi_{\text{in}}=3.04$ mm) by hot pressing at 200 °C. The complex permittivity and permeability values were measured in the 2–18 GHz frequency range by an Agilent N5230C network analyzer.

3. Results and discussion

The phase composition and structure of the as-prepared FeOOH/SiO₂ and the post-annealed samples were examined by XRD. The bottom spectrum in Fig. 1 shows the XRD pattern of the as-prepared FeOOH/SiO₂ sample. Compared with the data in reference,¹⁹ all the diffraction peaks can be indexed to the tetragonal structure of β -FeOOH (JCPDS No. 34-1266). No peaks from SiO₂ can be observed implying that the formed SiO₂ shell is amorphous phase. The upper spectrum is the XRD pattern of the post-annealed sample. In this pattern, the diffraction peaks well match both the magnetite Fe₃O₄ (JCPDS No. 87-0245) and the maghemite γ -Fe₂O₃ (JCPDS No. 39-1346). Because of the very similar patterns of γ -Fe₂O₃ and Fe₃O₄, it is difficult to distinguish the two phases by XRD analysis. Therefore, XPS characterization, which is sensitive to the oxidation state of the iron ions, was used to further confirm the crystal phase. Fig. 2 shows the Fe 2p core level XPS spectrum of the post-annealed sample, which has been charge corrected by the adventitious C 1s signal at 284.8 eV. It is known that the peaks for Fe₃O₄ generally shift to high binding energy and broaden due to the appearance of Fe²⁺, while the presence of the satellite peak at around 719.2 eV is the fingerprints of γ -Fe₂O₃.²⁰ For our sample, two broad peaks corresponding to Fe 2p_{3/2} and Fe 2p_{1/2} are located at 711.1 and 724.8 eV, respectively, which are higher than the standard values of 710.7 and 724.4 eV for γ -Fe₂O₃.²¹ No shakeup satellite peaks can be identified in the Fe 2p spectrum, thus excluding the presence of γ -Fe₂O₃ in the sample. In addition, the color of the final product changed to black from yellow after annealing treatment (shown in the inset of Fig. 2), which

also supports the phase transformation. Therefore, it is concluded that FeOOH core were completely transformed to pure Fe₃O₄ during the annealing process by controlling the annealing temperature, time and H₂/N₂ flow.

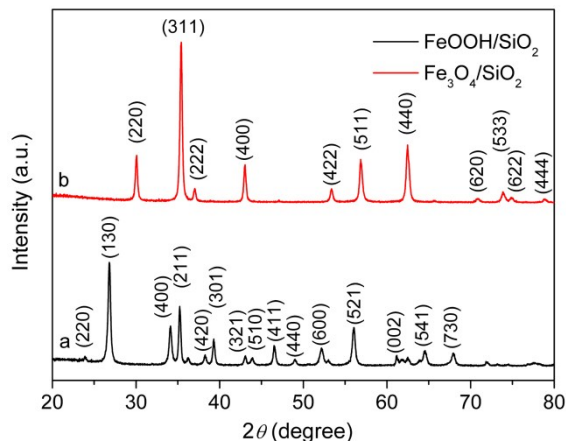


Fig. 1 XRD patterns of (a) as-prepared FeOOH/SiO₂ and (b) post-annealed samples (The main diffraction peaks were labeled as Fe₃O₄ phase).

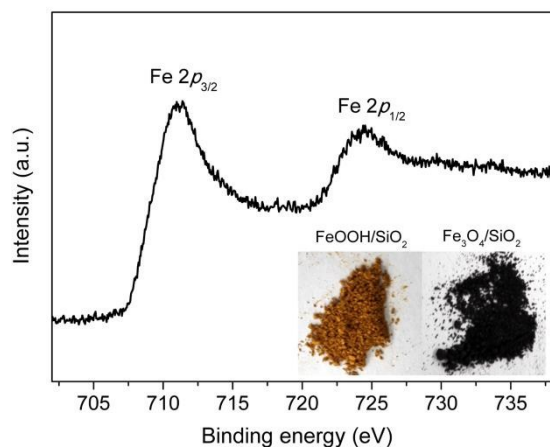


Fig. 2 Fe 2*p* core level XPS spectrum of the post-annealed sample. Inset: digital photographs of the FeOOH/SiO₂ (yellow) and Fe₃O₄/SiO₂ (black) powders.

Fig. 3 shows the SEM images of the as-prepared FeOOH/SiO₂ and Fe₃O₄/SiO₂ samples. Both of the samples exhibit rodlike shape with high aspect ratio, and no obvious morphology change occurred after annealing treatment. More detail observations of the morphology and size of the nanorods were carried out using TEM. Fig. 4a and b provide representative images of the as-prepared FeOOH/SiO₂ nanorods. As shown in Fig. 4a, the FeOOH/SiO₂ nanorods display monodispersed characteristic with the diameter and length in the range of 110–170 nm and 0.7–2.2 μm, respectively. The clear contrast in Fig. 4b confirms the core-shell structure of the individual FeOOH/SiO₂ nanorod. It is visible that a uniform SiO₂ layer with thickness of ~10 nm smoothly encapsulates the FeOOH rod. After annealing treatment in H₂/N₂ atmosphere, the FeOOH/SiO₂ nanorods were transformed into Fe₃O₄/SiO₂ nanorods, which have similar morphology and size as shown in Fig. 4c. However, it is clear in Fig. 4d that void space appears at the tip of the nanorod, and many pores distribute along the axis direction of the Fe₃O₄ core, which suggests the volume

shrinkage of the core owing to the phase transformation during the annealing process. Fig. 4e shows a high-resolution TEM image of the individual Fe₃O₄/SiO₂ nanorod. Clear lattice fringes are observed in the core regions, and the space between neighboring lattices is ~0.29 nm, corresponding to the (220) planes of Fe₃O₄. To investigate the dispersion of the Fe₃O₄/SiO₂ nanorods in PVDF, the fractured cross-section of the Fe₃O₄/SiO₂/PVDF nanocomposite was investigated by FESEM. In the inset of Fig. 4g, it is clear that the Fe₃O₄/SiO₂ nanorods remain 1D rodlike morphology in polymer after hot pressing at 200 °C. Corresponding elemental maps of the Fe, Si and F reveal the uniform dispersion of Fe₃O₄/SiO₂ nanorods in polymer, which may be helpful for enhancing the absorption properties. More interestingly, one can see from Fig. 4f that the Fe₃O₄/SiO₂/PVDF film is easily bended repeatedly and shows excellent flexibility. Thus, it is expected that the flexible Fe₃O₄/SiO₂/PVDF nanocomposite has potential applications in special materials and devices.

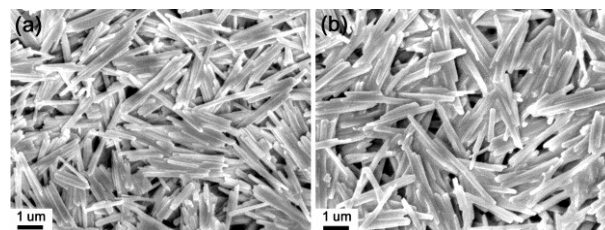


Fig. 3 FESEM images of (a) FeOOH/SiO₂ and (b) Fe₃O₄/SiO₂ samples.

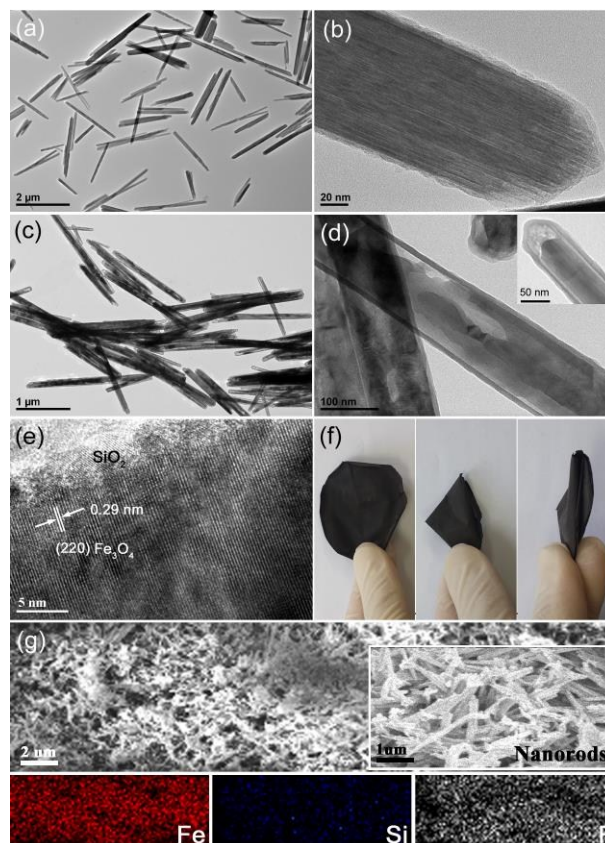


Fig. 4 (a) and (b) TEM images of FeOOH/SiO₂ nanorods, (c) and (d) TEM images of Fe₃O₄/SiO₂ nanorods, inset of (d): tip of Fe₃O₄/SiO₂ nanorods. (e) HRTEM image of individual Fe₃O₄/SiO₂ nanorod. (f) Digital photographs of the flexible

Fe₃O₄/SiO₂/PVDF film. (g) FESEM images of the fractured cross-section of the Fe₃O₄/SiO₂/PVDF nanocomposite and corresponding elemental maps of Fe, Si and F. Inset: enlarged image of the Fe₃O₄/SiO₂ nanorods in PVDF.

The field dependence of magnetization of the Fe₃O₄/SiO₂ sample was measured at room temperature, and presented in Fig. 5. Obvious hysteresis loop in the *M*–*H* curve indicates the ferromagnetic behavior of the Fe₃O₄/SiO₂ nanorods. The saturation magnetization (*M*_s) and coercivity (*H*_c) of the sample are 50.0 emu/g and 410.0 Oe, respectively. Compared with pure Fe₃O₄ nanowires or nanorods,^{13, 22, 23} the *M*_s of the Fe₃O₄/SiO₂ core-shell nanorods is slightly lower due to the presence of the nonmagnetic SiO₂ shells in the nanocomposite. Whereas the *H*_c value is much higher, suggesting the larger anisotropic energy which is beneficial for the enhancement of microwave absorption performance.

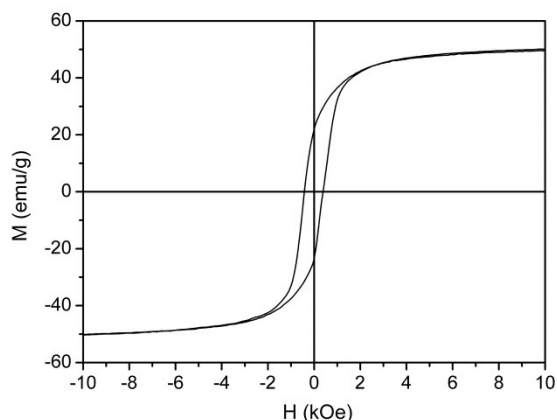


Fig. 5 Magnetization hysteresis loops of the Fe₃O₄/SiO₂ core-shell nanorods measured at room temperature.

Because of the special structure as shown above, the Fe₃O₄/SiO₂/PVDF nanocomposite may exhibit good microwave absorption properties. According to the transmission line theory, its absorption properties can be obtained based on the measured relative complex permittivity ($\epsilon_r = \epsilon' - j\epsilon''$) and relative complex permeability ($\mu_r = \mu' - j\mu''$).²⁴ The reflection loss (*R*_L) values were calculated by the following equations at a given frequency and thickness layer^{25, 26}

$$Z_{in} = \sqrt{\frac{\mu_r}{\epsilon_r}} \tanh \left[j \left(\frac{2\pi f d}{c} \right) \sqrt{\mu_r \epsilon_r} \right] \quad (1)$$

$$R = 20 \log \left| \frac{Z_{in} - 1}{Z_{in} + 1} \right| \quad (2)$$

where *Z*_{in} is the normalized input impedance, ϵ_r and μ_r are the complex permittivity and permeability of the composite absorber, respectively; *f* is the frequency; *d* is the thickness of the absorber, and *c* is the velocity of light in free space. Fig. 6a shows the *R*_L of the Fe₃O₄/SiO₂/PVDF nanocomposite with thickness varies from 1 to 5 mm in the frequency range of 2–18 GHz. It can be found that all the minimal *R*_L values are less than –10 dB for the nanocomposites with thicknesses of 2–5 mm, and the minimal *R*_L is down to –28.6 dB at 8.1 GHz as the thickness is 2.5 mm. At the same time, it is visible that two strong *R*_L peaks appear at high frequency and low frequency regions respectively, when the thickness of the absorbers is larger than 3 mm. The *R*_L peak at low frequency is a normal phenomenon in most magnetic absorbers, while the strong

absorbance at high frequency can be attributed to the increase of dielectric loss.¹⁰ The appearance of dual *R*_L peaks was also reported in Fe₃O₄/ZnO sphere decorated graphene (Fe₃O₄/ZnO/RGO).¹⁰ Compared with this previous result, the Fe₃O₄/SiO₂/PVDF nanocomposite can achieve stronger absorption in low frequency range whereas the Fe₃O₄/ZnO/RGO has better absorption ability in high frequency region. The dual *R*_L peaks are beneficial for extending the absorption bandwidth corresponding to *R*_L below –10 dB. Additionally, the *R*_L peaks have a tendency to shift from high frequency to low frequency with increasing the thickness. Consequently, the frequency range corresponding to effective absorption (*R*_L < –10 dB) can be tuned by changing the thicknesses of absorber. For example, the frequency range with *R*_L below –10 dB shifts from 17.6 to 3.3 GHz by decreasing the thickness from 2 to 5 mm. Since more than 90% of EM wave energy can be attenuated by the absorber when its *R*_L value is less than –10 dB,²⁷ the Fe₃O₄/SiO₂/PVDF nanocomposite is very promising for new types of microwave absorption materials.

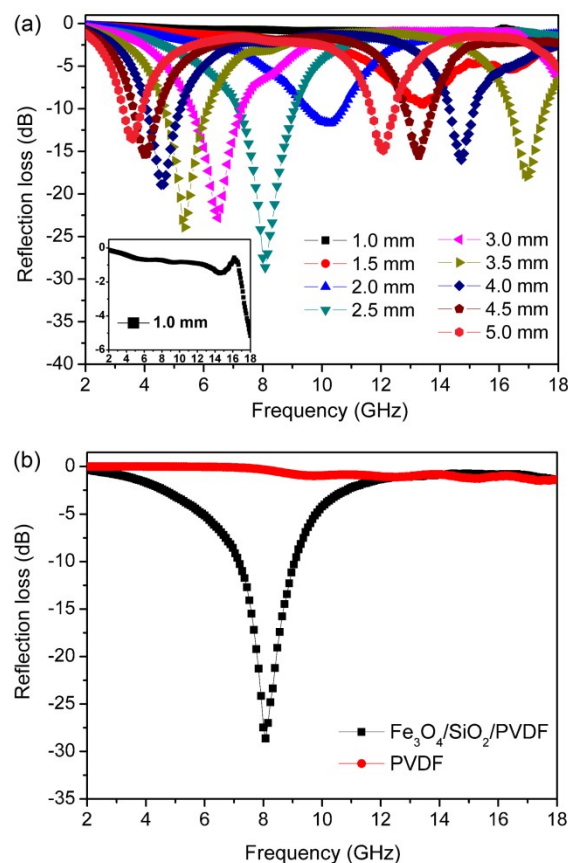


Fig. 6 (a) Reflection losses of the Fe₃O₄/SiO₂/PVDF nanocomposites with thickness of 1–5 mm, inset: *R*_L curve of the Fe₃O₄/SiO₂/PVDF nanocomposites with thickness of 1 mm; (b) Reflection losses of the Fe₃O₄/SiO₂/PVDF nanocomposite and pure PVDF with a thickness of 2.5 mm.

Furthermore, it is known that one of the drawbacks for Fe₃O₄ absorbers is the high density, which hampers the practical applications. Generally, the Fe₃O₄ should be added at least 50 wt.% in matrix for obtaining *R*_L value less than –20 dB. For our sample, the loading amount of Fe₃O₄/SiO₂ nanorods in the PVDF matrix is only 40 wt.%, and the minimum *R*_L is down

to -28.6 dB. Hence, the $\text{Fe}_3\text{O}_4/\text{SiO}_2/\text{PVDF}$ nanocomposite can be used as lightweight microwave absorbers with strong EM absorption properties. Since PVDF is a typical dielectric polymer, the attenuation of EM wave by PVDF matrix should also be considered. In Fig. 6b, we compare the reflection loss of the $\text{Fe}_3\text{O}_4/\text{SiO}_2/\text{PVDF}$ nanocomposite (2.5 mm) to that of pure PVDF (2.5 mm). It can be found that the pure PVDF shows very poor microwave absorption property over 2–18 GHz frequency range and the minimum R_L value is only -1.4 dB. Hence, the excellent microwave absorption performance of the $\text{Fe}_3\text{O}_4/\text{SiO}_2/\text{PVDF}$ composite should be assigned to the special structure as discussed in the following section.

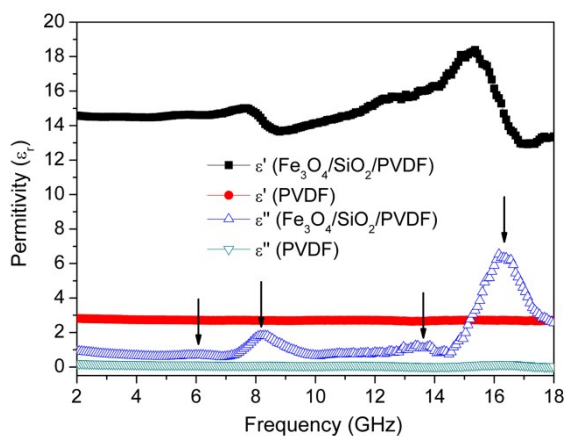


Fig. 7 The complex permittivities of $\text{Fe}_3\text{O}_4/\text{SiO}_2/\text{PVDF}$ nanocomposite and PVDF matrix.

Fe_3O_4 is a typical double-complex medium with dielectric loss and magnetic loss. To understand the possible microwave absorption mechanisms, the complex ϵ_r and μ_r of the $\text{Fe}_3\text{O}_4/\text{SiO}_2/\text{PVDF}$ nanocomposite and pure PVDF were shown and discussed below. Fig. 7 shows the real and imaginary parts of the complex permittivities over 2–18 GHz frequency range. For $\text{Fe}_3\text{O}_4/\text{SiO}_2/\text{PVDF}$ nanocomposite, the values of ϵ' are in the range of 13.0–18.6, while the values of ϵ'' vary from 0.5 to 6.8. Generally, the complex permittivities of Fe_3O_4 materials show frequency dispersion behavior, that is, ϵ_r decreasing with increasing frequency.^{5, 11, 28, 29} However, both the real part (ϵ') and imaginary part (ϵ'') of the $\text{Fe}_3\text{O}_4/\text{SiO}_2/\text{PVDF}$ nanocomposite fluctuate with increasing frequency, and exhibit several peaks which show resonant characteristics.⁵ Since the ϵ' of PVDF matrix keeps constant (~ 2.6) and ϵ'' approximates to zero in the whole frequency range, the unique dielectric behavior should be attributed to the special structure of the porous $\text{Fe}_3\text{O}_4/\text{SiO}_2$ core-shell nanorods. More interestingly, the ϵ'' curve of the $\text{Fe}_3\text{O}_4/\text{SiO}_2/\text{PVDF}$ nanocomposite possesses four resonance peaks, two weak resonance peaks at 6.0, 13.4 GHz and two strong resonant peaks at 8.2, 16.2 GHz. In most cases, there are only one or two resonant peaks in absorbers such as CuS ,³⁰ $\text{Fe}_3\text{O}_4/\text{CuSiO}_3$,² $\text{Fe}_3\text{O}_4/\text{C}$.³¹ The appearance of multiple resonant peaks in ϵ'' curve demonstrates multirelaxations in $\text{Fe}_3\text{O}_4/\text{SiO}_2/\text{PVDF}$ nanocomposite, which originate from multiple kinds of polarizations.³² Firstly, the dipole polarization in Fe_3O_4 can be generated due to the electrons transfer between Fe^{2+} and Fe^{3+} ions as EM wave applied. Secondly, interfacial polarization, which is also known as Maxwell-Wagner polarization, appears in a heterogeneous media consisting of components with different conductivity and permittivity.^{6, 33} As to $\text{Fe}_3\text{O}_4/\text{SiO}_2/\text{PVDF}$ nanocomposites, multi-interfaces including $\text{Fe}_3\text{O}_4\text{--SiO}_2$ and $\text{SiO}_2\text{--PVDF}$

interfaces are present, thus producing two kinds of interfacial polarizations as a result of the accumulation of charges at the heterointerfaces. In addition, as observed in TEM images, numerous pores and void spaces exist in the $\text{Fe}_3\text{O}_4/\text{SiO}_2$ nanocomposite. These pores and void spaces can also create interfacial electrical polarizations, providing extra relaxation processes.³⁴ The multirelaxations endow the $\text{Fe}_3\text{O}_4/\text{SiO}_2/\text{PVDF}$ nanocomposites high ϵ'' values, and particularly the ϵ'' value can reach 6.8 at 16.2 GHz, which implies the strong dielectric loss against EM wave in high frequency region.

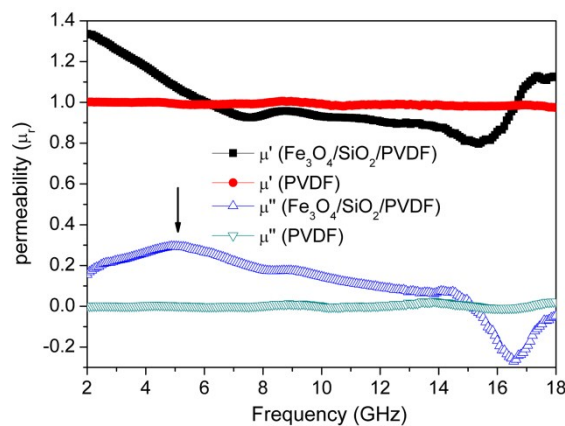


Fig. 8 The complex permeabilities of $\text{Fe}_3\text{O}_4/\text{SiO}_2/\text{PVDF}$ nanocomposite and PVDF matrix.

Fig. 8 presents the measurements of complex permeability versus frequency for $\text{Fe}_3\text{O}_4/\text{SiO}_2/\text{PVDF}$ nanocomposite and PVDF matrix. The values of real part (μ') and imaginary part (μ'') of PVDF matrix almost keep constant in the measured range, in which the magnitudes of μ' and μ'' are around 1 and 0, respectively. This suggests that the PVDF matrix has no contribution to the magnetic loss. For $\text{Fe}_3\text{O}_4/\text{SiO}_2/\text{PVDF}$ nanocomposite, the values of μ' are in the range of 0.78–1.35, and the variations of μ' successively display sharp decrease (2–7.5 GHz), slight fluctuation (7.5–15.5 GHz), and large increase (15.5–18 GHz) with increasing frequency. The μ'' curve exhibits a broad resonance from 2 to 8 GHz accompanied by a quick decline in subsequent 9–18 GHz. It is visible that the μ'' values are higher than 0.1 in the frequency region over 2–12.2 GHz, indicating the large magnetic loss in low frequency range in $\text{Fe}_3\text{O}_4/\text{SiO}_2/\text{PVDF}$ nanocomposite. For magnetic materials, the magnetic loss mainly derives from hysteresis, domain wall resonance, natural resonance and eddy current effect.³⁵ Nevertheless, the hysteresis loss is negligible in the weak field, and the domain wall resonance loss commonly occurs at MHz frequency.³⁶ Hence, the natural resonance and eddy current effect may be responsible for the attenuation of electromagnetic waves over 2–18 GHz frequency range. The natural resonance for the $\text{Fe}_3\text{O}_4/\text{SiO}_2/\text{PVDF}$ nanocomposite is evidenced by the presence of resonance peak in permeability (μ'') curve. According to the natural-resonance equations³⁷

$$2\pi f_r = rH_a \quad (3)$$

$$H_a = 4|K_1|/3\mu_0 M_s \quad (4)$$

where r is the gyromagnetic ratio, H_a is the anisotropy field, and $|K_1|$ is the anisotropy coefficient, M_s is the saturation magnetization. The resonance frequency strongly depends on the effective anisotropy field H_a , which is associated with the magneto-crystalline anisotropy and shape anisotropy of the

sample. For bulk Fe_3O_4 with small magneto-crystalline anisotropy, the resonance frequency (f_r) of Fe_3O_4 is usually below 1.5 GHz,³¹ much lower than the f_r of the $\text{Fe}_3\text{O}_4/\text{SiO}_2/\text{PVDF}$ nanocomposite (~ 5 GHz). Such resonance shift to high frequency can be ascribed to the large shape anisotropy which arises from the special 1D structure and porous feature of the $\text{Fe}_3\text{O}_4/\text{SiO}_2$ nanorods. Eddy current effect is another possible factor for EM wave absorption. The eddy current loss can be expressed by³⁶

$$\mu'' = 2\pi\mu_0(\mu')^2\sigma \cdot d^2 f/3 \quad (5)$$

where μ_0 and σ are the electric permeability and the conductivity in vacuum, respectively. If the magnetic loss results from eddy current loss, the values of $\mu''(\mu')^{-2}f^{-1}$ are constant when the frequency is varied. As observed in Fig. 9, the values show serious fluctuations in the 2–18 GHz frequency range, implying that the eddy current effect has no significant effect on the EM wave absorption.

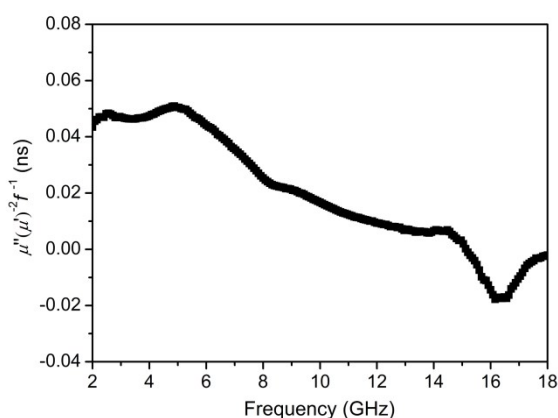


Fig. 9 The frequency dependence of $\mu''(\mu')^{-2}f^{-1}$ for $\text{Fe}_3\text{O}_4/\text{SiO}_2/\text{PVDF}$ nanocomposite.

From the above results, it can be found that both dielectric loss and magnetic loss contribute to the excellent microwave absorption performance of the $\text{Fe}_3\text{O}_4/\text{C}/\text{PVDF}$ nanocomposite. The dielectric loss and magnetic loss can be evaluated by the dielectric tangent loss ($\tan \delta_e = \epsilon''/\epsilon'$) and magnetic tangent loss ($\tan \delta_m = \mu''/\mu'$), as displayed in Fig. 10. It is clear that the magnetic loss with the $\tan \delta_m$ values of 0.06–0.28 is dominant at low frequency range (2–14.7 GHz), whereas the dielectric loss with the maximum $\tan \delta_e$ of 0.45 becomes important at high frequency range (14.7–18 GHz). The efficient complementarities between the two losses can facilitate the entrance of incident EM wave into absorbers which would benefit the absorption property of the nanocomposite.^{38, 39} Therefore, the unique structural characters and the synergetic effect between multiple components are fundamental to the enhanced microwave absorption properties of the $\text{Fe}_3\text{O}_4/\text{C}/\text{PVDF}$ nanocomposites. The strong microwave absorption ability is assigned to the high magnetic loss, high dielectric loss and the good impedance matching. Additionally, multiple scattering of incident EM wave can occur at the pores/void spaces in the $\text{Fe}_3\text{O}_4/\text{SiO}_2$ nanorods as well as the interfaces between nanorods and matrix, which provide extra approaches to attenuating EM wave.³⁴ The synthesized $\text{Fe}_3\text{O}_4/\text{C}/\text{PVDF}$ nanocomposite absorbers combining strong absorption, light weight, antioxidation and excellent flexibility can be considered as a promising absorber in practical applications.

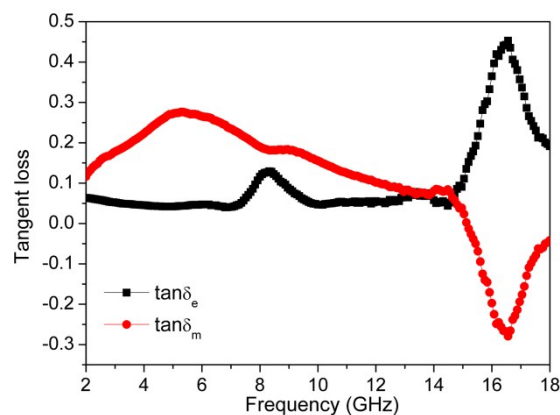


Fig. 10 The dielectric tangent loss and magnetic tangent loss of the $\text{Fe}_3\text{O}_4/\text{SiO}_2/\text{PVDF}$ nanocomposite.

4. Conclusions

In summary, one dimensional $\text{Fe}_3\text{O}_4/\text{SiO}_2$ nanorods with core-shell and porous structures were successfully synthesized by a wet-chemical method. And the $\text{Fe}_3\text{O}_4/\text{SiO}_2/\text{PVDF}$ nanocomposites were fabricated with blending and hot press approaches for microwave absorption applications. The $\text{Fe}_3\text{O}_4/\text{SiO}_2/\text{PVDF}$ nanocomposite (filler content of 40 wt.%) exhibits excellent microwave absorption properties over 2–18 GHz due to the special structure features as well as the synergetic effect between the multiple components. The minimum R_L value reaches -28.6 dB at 8.1 GHz for the absorber with the thickness of 2.5 mm. The flexible property of the $\text{Fe}_3\text{O}_4/\text{SiO}_2/\text{PVDF}$ nanocomposite is still kept as that of pure PVDF, which make the nanocomposite useful in many special fields. We believe that the $\text{Fe}_3\text{O}_4/\text{SiO}_2/\text{PVDF}$ nanocomposite is a good candidate for high-performance microwave absorbers with strong absorption, lightweight, antioxidation and flexibility, which are promising for applications in commercial and military fields. Additionally, the facile synthesis strategy can be easily extended to design other high-performance microwave absorbers.

Acknowledgements

This work was supported by the National Natural Science Foundation of China (No. 51102006 and 51472012), Beijing Municipal Science and Technology Project (No. D14110300240000), and the Fundamental Research Funds for the Central Universities.

Notes and references

^aSchool of Materials Science and Engineering, Beihang University, Beijing 100191, China.

^bSchool of Chemistry and Environment, Beihang University, Beijing 100191, China. Fax: +86-10-82316066; Tel: +86-10-82316066; E-mail: wanggsh@buaa.edu.cn

† Electronic Supplementary Information (ESI) available: details of any supplementary information available should be included here. See DOI: 10.1039/b000000x/

1. X. M. Meng, X. J. Zhang, C. Lu, Y. F. Pan and G. S. Wang, *J. Mater. Chem. A*, 2014, **2**, 18725-18730.
2. J. J. Xu, J. W. Liu, R. C. Che, C. Y. Liang, M. S. Cao, Y. Li and Z. W. Liu, *Nanoscale*, 2014, **6**, 5782-5790.

3. C. Y. Liang, C. Y. Liu, H. Wang, L. N. Wu, Z. H. Jiang, Y. J. Xu, B. Z. Shen and Z. J. Wang, *J. Mater. Chem. A*, 2014, **2**, 16397-16402.
4. J. W. Liu, R. C. Che, H. J. Chen, F. Zhang, F. Xia, Q. S. Wu and M. Wang, *Small*, 2012, **8**, 1214-1221.
5. M.-S. Cao, J. Yang, W.-L. Song, D.-Q. Zhang, B. Wen, H.-B. Jin, Z.-L. Hou and J. Yuan, *ACS Appl. Mater. Inter.*, 2012, **4**, 6948-6955.
6. H. Yang, M. Cao, Y. Li, H. Shi, Z. Hou, X. Fang, H. Jin, W. Wang and J. Yuan, *Adv. Opt. Mater.*, 2014, **2**, 214-219.
7. J. P. Zou, Z. Z. Wang, M. Q. Yan and H. Bi, *J. Phys. D Appl. Phys.*, 2014, **47**, 275001.
8. X. A. Li, B. Zhang, C. H. Ju, X. J. Han, Y. C. Du and P. Xu, *J. Phys. Chem. C*, 2011, **115**, 12350-12357.
9. J. W. Liu, J. Cheng, R. C. Che, J. J. Xu, M. M. Liu and Z. W. Liu, *J. Phys. Chem. C*, 2013, **117**, 489-495.
10. D. P. Sun, Q. Zou, Y. P. Wang, Y. J. Wang, W. Jiang and F. S. Li, *Nanoscale*, 2014, **6**, 6557-6562.
11. B. Zhang, Y. C. Du, P. Zhang, H. T. Zhao, L. L. Kang, X. J. Han and P. Xu, *J. Appl. Polym. Sci.*, 2013, **130**, 1909-1916.
12. H. M. Zhang, C. L. Zhu, Y. J. Chen and H. Gao, *Chemphyschem*, 2014, **15**, 2261-2266.
13. A. G. Yan, Y. J. Liu, Y. Liu, X. H. Li, Z. Lei and P. T. Liu, *Mater. Lett.*, 2012, **68**, 402-405.
14. H. J. Wu, G. L. Wu and L. D. Wang, *Powder Technol.*, 2015, **269**, 443-451.
15. D. P. Sun, Q. Zou, G. Q. Qian, C. Sun, W. Jiang and F. S. Li, *Acta Mater.*, 2013, **61**, 5829-5834.
16. S. He, G.-S. Wang, C. Lu, J. Liu, B. Wen, H. Liu, L. Guo and M.-S. Cao, *J. Mater. Chem. A*, 2013, **1**, 4685-4692.
17. X.-J. Zhang, G.-S. Wang, W.-Q. Cao, Y.-Z. Wei, J.-F. Liang, L. Guo and M.-S. Cao, *ACS Appl. Mater. Inter.*, 2014, **6**, 7471-7478.
18. N. Hijnen and P. S. Clegg, *Chem. Mater.*, 2012, **24**, 3449-3457.
19. M. B. Blesa and E. Matijevic, *Adv. Colloid Interface Sci.*, 1989, **29**, 173.
20. T. Fujii, F. de Groot, G. Sawatzky, F. Voogt, T. Hibma and K. Okada, *Phys. Rev. B*, 1999, **59**, 3195.
21. G. B. Sun, B. X. Dong, M. H. Cao, B. Q. Wei and C. W. Hu, *Chem. Mater.*, 2011, **23**, 1587-1593.
22. J. X. Wan, X. Y. Chen, Z. H. Wang, X. G. Yang and Y. T. Qian, *J. Cryst. Growth*, 2005, **276**, 571-576.
23. J. Wang, Y. J. Wu and Y. J. Zhu, *Mater. Chem. Phys.*, 2007, **106**, 1-4.
24. H. Wang, L. N. Wu, J. F. Jiao, J. G. Zhou, Y. J. Xu, H. Y. Zhang, Z. H. Jiang, B. Z. Shen and Z. J. Wang, *J. Mater. Chem. A*, 2015, **3**, 6517-6525.
25. M. S. Cao, X. L. Shi, X. Y. Fang, H. B. Jin, Z. L. Hou, W. Zhou and Y. J. Chen, *Appl. Phys. Lett.*, 2007, **91**, 203110.
26. G. S. Wang, L. Z. Nie and S. H. Yu, *RSC Adv.*, 2012, **2**, 6216-6221.
27. G. Z. Wang, X. G. Peng, L. Yu, G. P. Wan, S. W. Lin and Y. Qin, *J. Mater. Chem. A*, 2015, **3**, 2734-2740.
28. X. Sun, J. P. He, G. X. Li, J. Tang, T. Wang, Y. X. Guo and H. R. Xue, *J. Mater. Chem. C*, 2013, **1**, 765-777.
29. M. Zong, Y. Huang, Y. Zhao, X. Sun, C. H. Qu, D. D. Luo and J. B. Zheng, *RSC Adv.*, 2013, **3**, 23638-23648.
30. S. He, G. S. Wang, C. Lu, X. Luo, B. Wen, L. Guo and M. S. Cao, *Chemphyschem*, 2013, **78**, 250-258.
31. Y. J. Chen, G. Xiao, T. S. Wang, Q. Y. Ouyang, L. H. Qi, Y. Ma, P. Gao, C. L. Zhu, M. S. Cao and H. B. Jin, *J. Phys. Chem. C*, 2011, **115**, 13603-13608.
32. Y. J. Chen, F. Zhang, G. G. Zhao, X. Y. Fang, H. B. Jin, P. Gao, C. L. Zhu, M. S. Cao and G. Xiao, *J. Phys. Chem. C*, 2010, **114**, 9239-9244.
33. B. D. Bertram and R. A. Gerhardt, *J. Am. Ceram. Soc.*, 2011, **94**, 1125-1132.
34. B. Shen, W. T. Zhai, M. M. Tao, J. Q. Ling and W. G. Zheng, *ACS Appl. Mater. Interfaces*, 2013, **5**, 11383-11391.
35. Y. C. Du, W. W. Liu, R. Qiang, Y. Wang, X. J. Han, J. Ma and P. Xu, *ACS Appl. Mater. Inter.*, 2014, **6**, 12997.
36. M. Z. Wu, Y. D. Zhang, S. Hui, T. D. Xiao, S. H. Ge, W. A. Hines, J. I. Budnick and G. W. Taylor, *Appl. Phys. Lett.*, 2002, **80**, 4404-4406.
37. C. Kittel, *Phys. Rev. B*, 1948 **73** 155.
38. Y. J. Chen, P. Gao, R. X. Wang, C. L. Zhu, L. J. Wang, M. S. Cao and H. B. Jin, *J. Phys. Chem. C*, 2009, **113**, 10061-10064.
39. M. S. Cao, R. R. Qin, C. J. Qiu and J. Zhu, *Mater. Design.*, 2003, **24**, 391-396.

Graphical abstract

- (1) The novel $\text{Fe}_3\text{O}_4/\text{SiO}_2/\text{PVDF}$ composite by embedding $\text{Fe}_3\text{O}_4/\text{SiO}_2$ porous nanorods in polyvinylidene fluoride (PVDF) matrix.
- (2) The $\text{Fe}_3\text{O}_4/\text{SiO}_2/\text{PVDF}$ nanocomposite with filler content of 40 wt.% shows excellent microwave absorption performance over 2–18 GHz, and the minimum reflection loss (RL) can reach -28.6 dB as the thickness is 2.5 mm.

